INSTITUTE OF PHYSICS PUBLISHING PLASMA SOURCES SCIENCE AND TECHNOLOGY

Plasma Sources Sci. Technol. **16** (2007) 233–239 doi:10.1088/0963-0252/16/2/004

Laser interferometry measurements of a high density propagating current sheet

J W Berkery[1], T E Markusic[2] and E Y Choueiri

Electric Propulsion and Plasma Dynamics Laboratory (EPPDyL), Princeton University, Princeton, NJ 08544, USA

E-mail: choueiri@princeton.edu

Received 25 October 2006, in final form 14 December 2006
Published 5 February 2007
Online at stacks.iop.org/PSST/16/233

Abstract

A helium–neon laser Mach–Zehnder quadrature interferometer is used to measure the electron number density in a propagating current sheet. In some cases the density rise rate was too high to be resolved by the system. Otherwise, the interferometer is used to measure time-resolved density at a particular location in the accelerator. The location of the beam is then moved between shots and, because of the repeatability of the discharge, multiple shots can be pieced together to create a temporally and spatially resolved view of the evolution of the sheet and of a wake of plasma that is left behind the sheet. The measurements confirm an emerging picture of the evolution of these structures that is based on high-speed photographs and current density measurements. They also reveal that the wake originates out of a bifurcation of the current sheet and that it is of comparable density to the sheet.

1. Introduction

An electromagnetic pulsed plasma thruster (PPT) is a type of electric space propulsion device that accelerates gaseous propellants to a high velocity in a sheet of current. PPTs are candidates for satellite attitude control or constellation positioning because they can deliver small impulse bits at high specific impulse. The dynamics of the current sheet must be well understood in order to identify means of improving thruster performance. One source of thrust inefficiency is the tendency of mass to leak out of the current sheet and into a wake [1]. The present work describes the use of a helium–neon laser interferometer to determine the time-resolved electron number density in a propagating high density current sheet and in its wake.

Helium–neon laser interferometers have been used in pulsed plasma applications such as the field-reversed configuration [2], z-pinch [3], spheromak [4] and plasma opening switch [5]. The plasma source used here is very repeatable [6] in that it produces current sheets that behave very similarly from shot to shot. Instead of merely a single point or chord measurement of density, measurements from multiple discharges can be pieced together to create a spatial and temporal map of the density. This is accomplished by using a movable mirror assembly to change the position of the laser beam inside the vacuum tank between shots.

We have previously reported measurements of electron number density at single locations with time resolution [1, 7]. Also, photographic and magnetic measurements that show the evolution of the current sheet's light emission and magnetic field (and hence current density) have been previously reported [6]. The photographs showed the existence of a canted current sheet and a wake of plasma travelling at a lower velocity along the cathode. The current density measurements showed that the current was carried in the canted sheet but not in the wake. Single point measurements of the density showed that the wake structure was of significant density compared with the sheet. For the first time we now present spatially and temporally resolved measurements of the electron density in the current sheet and the wake.

First, we briefly describe the experimental apparatus. Then an overview of the theory of interferometry pertaining to our setup is presented. And then the particular interferometry system, including the components and setup, is described. The analysis of the data is discussed next, including a particular error of the phase detection system resulting from high density rise rates. Finally, the experimental measurements are presented and discussed.

[1] Present address: Department of Applied Physics and Applied Mathematics, Columbia University, New York, NY 10027, USA.
[2] Present address: Space Exploration Technologies, El Segundo, CA 90245, USA.

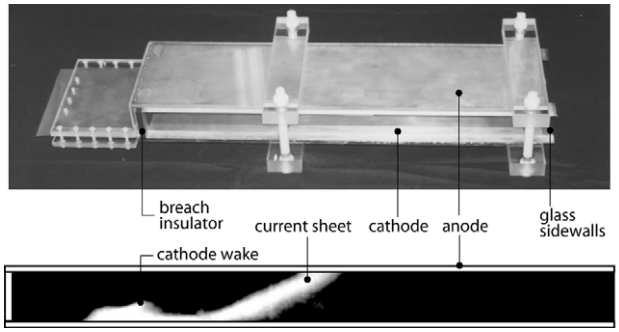

Figure 1. Photograph (top) of the discharge chamber and (bottom) photograph of the discharge near the midsection of the accelerator (argon, 75 mTorr).

2. Experimental apparatus

The experimental apparatus used in this study has been described in detail previously [7]. It is a parallel plate accelerator that uses a pulse forming network to pulse a high current (∼60 kA for ∼25 μs) through a uniform pre-fill of propellant gas (75–400 mTorr). The anode and cathode are 60 cm × 15 cm copper plates separated by 5 cm tall, 2.5 cm wide Pyrex sidewalls. Photographs of the accelerator and a discharge are shown in figure 1. The propagation direction of the current sheet (to the right in the discharge photograph) is x, the direction of the electrode separation is y and the direction out of the page in the discharge photograph is z.

A typical discharge in our apparatus proceeds as follows (more detailed descriptions can be found elsewhere [1, 7]). As the current rises, a discharge is struck at the breach of the accelerator. This forms into a thin sheet of current which proceeds to propagate due to the interaction of the current and its own magnetic field. As the sheet sweeps up propellant gas it begins to cant so that the anode attachment is leading the cathode attachment. A wake of plasma then forms behind the current sheet. Finally, the fully ionized current sheet propagates at a constant canting angle and velocity (≈4 cm μs^{-1}) and the wake moves at a slower velocity along the cathode, growing in length. Figure 1 (bottom) shows a typical discharge that has entered this final phase of propagation.

A unique feature of this parallel plate accelerator is that it has Pyrex sidewalls that allow good optical access. Also, the discharge is both uniform in the z direction and is very repeatable. All these features make laser interferometry very convenient. The interferometer beam goes through the glass sidewalls and allows measurement of the electron number density at a particular location in x and y with time resolution. The beam location can then be moved, and multiple shots can be displayed together to make a spatial map. These measurements will be shown in section 6.

3. Interferometry theory

The helium–neon (HeNe) laser interferometer [5,8–10] described in this article is used to measure the electron number density in a high density ($n_e \sim 10^{22}$ m^{-3}) pulsed plasma. Because the speed of propagation of the current sheet is high, the time scale of the measurement is small enough to consider the optics effectively stationary. Therefore neglecting the path length variations due to vibrations of the optics is a good assumption.

Assuming, then, that the plasma is uniform in the path of the laser beam, the phase change due to the index refraction of the plasma is given by

$$\Delta\phi = \frac{\omega}{c}(1 - n_f)l, \tag{1}$$

where ω is the laser frequency, n_f is the index of refraction and l is the path length of the laser beam in the plasma. Under the condition that ω_p, ω_c and ν_{ei} are each much less than ω, the expression for the index of refraction is greatly simplified to the form

$$n_f = 1 - \frac{\omega_p^2}{2\omega^2}. \tag{2}$$

For a HeNe laser interferometer with a wavelength of 632.8 nm, these equations reduce to

$$n_e = 5.61 \times 10^{20}\frac{\Delta\phi}{l}, \tag{3}$$

with l in metres, $\Delta\phi$ in radians and n_e in m^{-3}. In the apparatus used in the present experiments, the length l is the 10 cm width between the Pyrex sidewalls.

4. Helium–neon interferometer

The interferometer described here is a Mach–Zehnder heterodyne laser interferometer with an electronic quadrature phase detection. In the present experiment, phase differences between the two laser beam paths arise when plasma propagates rapidly through the scene beam. By measuring the phase change of the scene beam with respect to the reference beam we can determine the electron number density of the plasma.

Two problems arise in the interpretation of data obtained with a conventional Mach–Zehnder interferometer: amplitude variations in the detected signal which arise from the attenuation or refractive bending in the plasma must be distinguished from phase variations, and, in general, it is not possible to determine the direction of the phase change (i.e. positive phase changes cannot be distinguished from negative ones). These problems are eliminated by using a heterodyne light source and quadrature phase detection. This is accomplished with a quadrature phase detector that uses two double balanced mixers to produce output signals proportional to the sine and cosine of the instantaneous phase and hence, unambiguously determines the quadrant of the phase angle. A schematic of the phase detection circuitry is shown in figure 2.

4.1. Resolution, sensitivity and frequency response

The spatial resolution of the interferometer is limited by the beam diameter of the laser used. In our case, this is approximately 3 mm.

We have, based simply on signal-to-noise ratio considerations, estimated the minimal resolvable variation in electron density in our device to be on the order of 10^{20} m^{-3}.

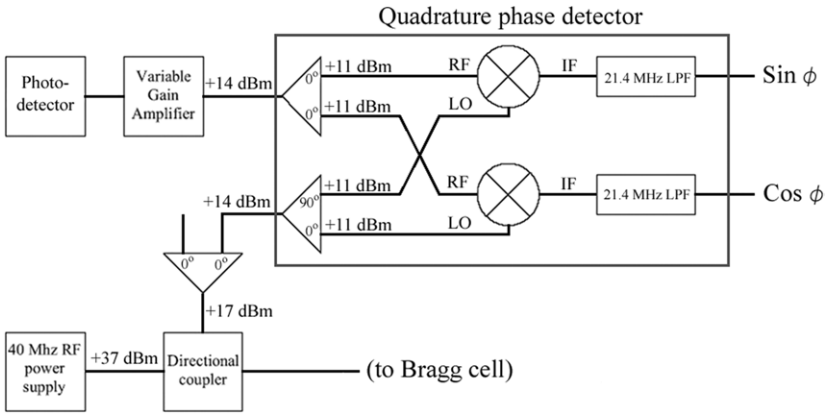

Figure 2. Schematic of the interferometer quadrature phase detection circuitry.

This could be improved, however, by using multiple passes through the plasma [11].

On the low frequency end, the interferometer is only useful for diagnosing plasmas that are fast enough so that we may consider the optics to be stationary. The phase variations measured by the detector due to room vibrations and atmospheric fluctuations alone reduce the useful time scale of the device to experiments which last less than 100 μs.

On the high frequency end, the low pass filters used in the phase detection circuit, limit the frequency response to about 10 MHz. Differentiating equation (3) with respect to time and using $l = 0.1$ m, $\Delta\phi \approx 2\pi$ and $1/\Delta t \approx 10$ MHz, we find the maximum resolvable temporal variation in electron density to be about 3.5×10^{29} m^{-3} s^{-1}. As will be shown later, this limit was exceeded in some measurements near the cathode of our experiment. The complications which resulted are described in section 5.1. Interestingly, increasing l increases the sensitivity of the interferometer but inhibits its ability to resolve quick rises in electron density.

4.2. *Components and setup*

In this subsection we will describe our particular setup of the laser interferometer, describing the equipment used and the layout of the instrument (see figure 3). This setup was previously described briefly in [7].

A Coherent 31-2108 17 mW HeNe laser is used to produce a beam that is first directed into a IntraAction AOM-405 acousto-optic cell driven by an IntraAction ME-40 40 MHz, 5 W RF power source (labelled 'Bragg cell' in figure 3). This splits the beam and adds a 40 MHz phase difference between the scene and reference beams. Because the pulsed plasma experiment produces a large amount of electromagnetic noise, all the electronics, including the laser, were housed in a Faraday cage.

Once the two beams leave the acousto-optic cell, they must be physically sent on different paths. Standard optical components (aluminized mirrors, dielectric beam splitters and anti-reflection windows) were used to steer the beams.

The scene beam is directed into the vacuum tank and onto a moving mirror assembly (figure 4). The four mirrors attached to the moving structure steer the beam through the glass sidewalls, while keeping it perpendicular to the direction of current sheet motion, x. Moving the assembly moves the beam between shots to probe a new location in x. To raise or lower the beam location (in y), it was necessary to enter the vacuum tank and realign the mirrors.

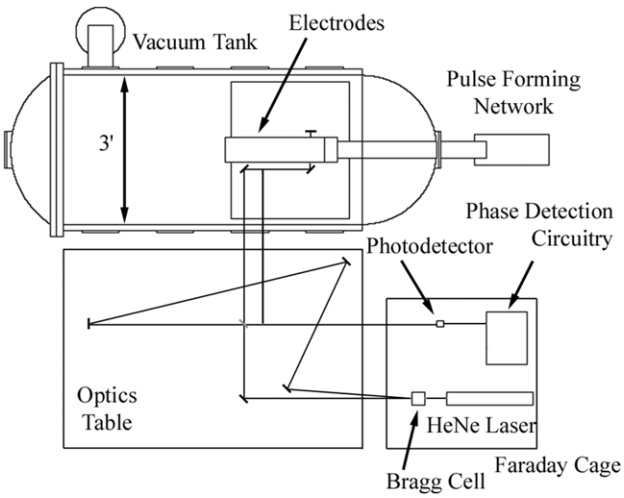

Figure 3. Schematic of the laser interferometry layout. The moving mirror assembly that directs the beam inside the vacuum tank is shown in figure 4 in more detail.

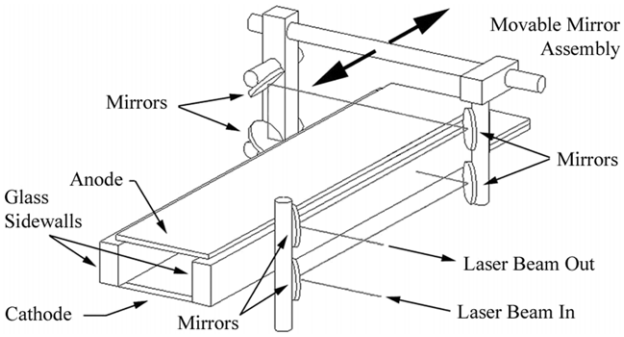

Figure 4. A schematic of the moving mirror assembly.

The reference beam, meanwhile, is sent on a path around the optic table that is approximately equal in length to the path length of the scene beam, within the tolerance of the coherence length of the laser. Because the moving mirror assembly changes the scene beam path length slightly, the path

length of the reference beam must be occasionally adjusted to compensate.

Once the scene beam leaves the vacuum tank, it is recombined with the reference beam by a 50/50 beam-splitter such that each beam loses half of its intensity. The recombined beam is directed onto the Thor Lab PDA155 detector. A 632.8 nm line filter allows only the laser light to be detected and a lens concentrates the light on the small area detector.

When the scene and reference beams are properly coaligned, they interfere, producing a sinusoidal 40 MHz beat wave at the detector. Using a variable gain amplifier, this signal is matched in amplitude with the 40 MHz signal from the power supply. These two signals are used as inputs, and mixed, in the 'quadrature phase detector' of figure 2. The output signals of the phase detection circuitry are the sine and cosine of the phase. The conversion of these signals to electron number density is discussed in the section below.

5. Analysis of data

This section describes the procedure for transforming the raw data from the phase detection circuitry into electron density profiles. The output from the quadrature phase detection circuitry is the instantaneous sine and cosine of the phase. Then, the instantaneous phase angle is given by

$$\phi = \arctan\left(\frac{\sin\phi}{\cos\phi}\right). \tag{4}$$

Figure 5 shows an example of the construction of an electron density profile from the raw output of the quadrature phase detector. In figure 5(*a*) the raw detector sine and cosine signals are plotted. Figure 5(*b*) shows the phase, which results from applying equation (4) to the waveforms in figure 5(*a*). The phase ranges between $-\pi \leqslant \phi \geqslant \pi$. As the phase changes it discontinuously jumps as it crosses the polar axis ($\phi = \pm\pi$). Since we are interested in the total phase change rather than the instantaneous phase angle, the individual segments (which are delineated by the sharp discontinuities) must be 'stacked' in a manner that respects the direction of the phase change. This is done by noting the slope of the phase just before the jump: positive pre-jump slope corresponds to increasing phase, negative pre-jump slope corresponds to decreasing phase. When the individual segments are properly stacked and the initial phase is subtracted out (this essentially removes the initial 'dc offset'), the resulting waveform can be input into equation (3) to yield the desired electron density profile, as shown in figure 5(*c*).

5.1. Phase error resulting from high density rise rates

When the electron density rise rates ($\mathrm{d}n_\mathrm{e}/\mathrm{d}t$) are especially steep (as is the case near the cathode in the present study), the phase jumps described in the example above can occur at a rate that is comparable to or greater than the laser modulation frequency. In this case, the detector can completely fail to record one or more of the positive-going phase jumps as the phase vector 'winds up'. When the phase vector 'unwinds' on the backside of the current sheet (which usually has less severe density gradients), the number of recorded negative-going phase jumps can be greater than the number of recorded positive-going phase jumps. As a result, when the segments are stacked to construct the total phase change waveform, the post-current-sheet phase will not return to the pre-current-sheet value as described in the example above but, rather, it will relax to a negative value, which is clearly unphysical. This is illustrated in figure 6.

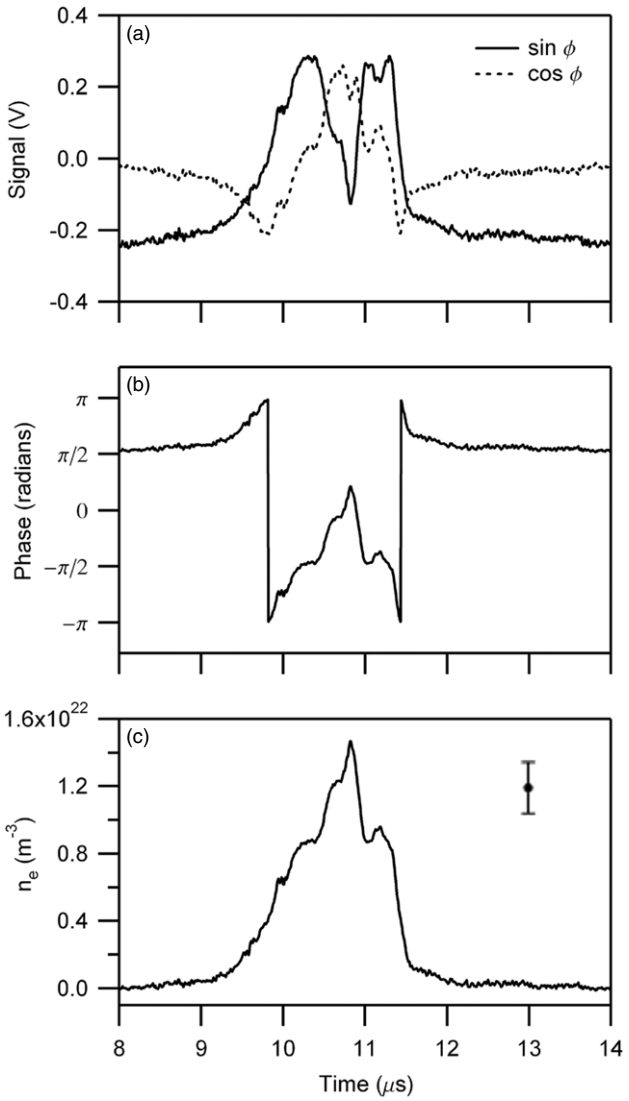

Figure 5. Construction of an electron density profile from raw phase detector output (argon, 100 mTorr): (*a*) raw quadrature phase detector output, (*b*) phase and (*c*) electron density. A typical error bar (based mainly on the repeatability of the peak density measurements) is also shown in panel (*c*).

It is possible to correct this phase detection issue by increasing the frequency response of the device. To do this, the modulation frequency must be increased. In addition to requiring a new acousto-optic cell and RF power supply, this would involve replacing many of the frequency sensitive components in the phase detector circuitry as well.

6. Experimental measurements

The electron number density versus time has been measured for a variety of experimental conditions, including various

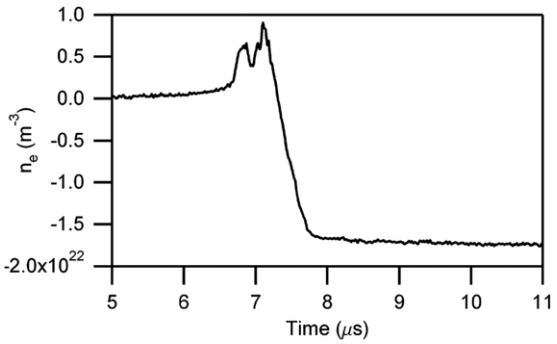

Figure 6. Example of a case where dn_e/dt exceeded the frequency response of the phase detector (argon, 100 mTorr).

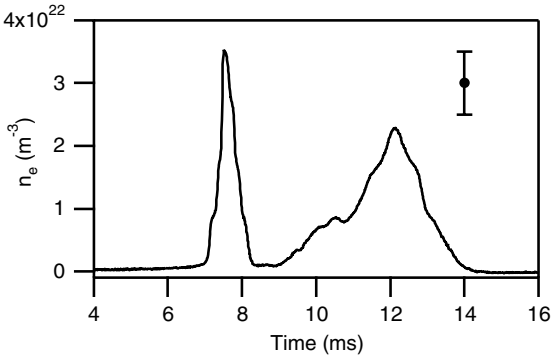

Figure 7. Example of measurement of electron number density versus time at a single location in the accelerator ($j = 3, i = 34$ in figure 8).

propellant gases and pressures, at a single location [1] or simultaneously in two locations [7] in the accelerator. An example is shown in figure 7.

While these measurements provide valuable insight into the trends of performance of the device under different operating conditions [1], they do not illustrate the development of the current sheet and wake structures. To get a better understanding of the dynamics of the sheet and wake, we have constructed a two-dimensional map of the density with time resolution. This was achieved by making many measurements over many shots at the same condition and moving the laser beam (or a magnetic field probe) between shots. This method has been used before to create contour plots of the density in a plasma opening switch [5] and in a similar fashion with magnetic field probes in the present experiment to create contours of current density [6, 7].

An array of measurement points is shown in figure 8. Rows $j = 1$–6 are, respectively, spaced at the following distances from the cathode (the bottom electrode) in the 5.08 cm gap: 0.48 cm, 1.27 cm, 2.06 cm, 3.02 cm, 3.81 cm and 4.60 cm. The horizontal spacing (x direction), starting with $i = 1$ at 0.32 cm from the breech, was constant thereafter at 0.635 cm. For the current density measurements, two magnetic probes were used per shot, eventually covering the entire array of 432 points. An example of contour plot of current density is shown in figure 9. This map was made by taking the value of the magnetic field at each location at time $t = 3\ \mu$s and taking the curl of the magnetic field data to obtain the current density.

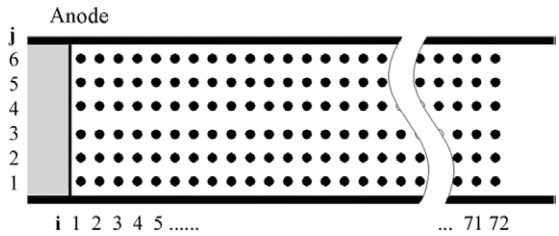

Figure 8. The array of measurement points in the accelerator is shown. The anode is on top, the cathode on bottom. An insulator backplate is shown (shaded).

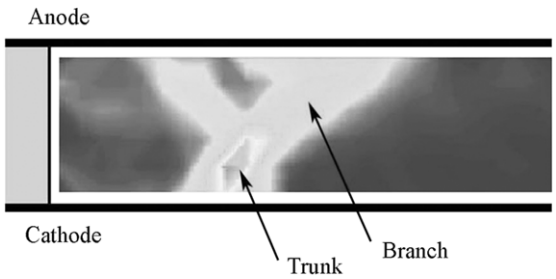

Figure 9. Current density contour at 3 μs, showing the branch and trunk structures.

It was surmised from the current density contours that the initial current sheet bifurcates, with a branch structure moving ahead along the anode of the trunk structure that is attached to the cathode [7]. The remnant of the initial sheet is visible to the left in figure 9 and is still carrying some current at this early point in the sheet evolution. However, it was seen that as time progresses the remnant of the sheet detaches from the anode and stops carrying current. In the current density contours this part of the structure disappears and the only structure left that carries current is the canted sheet. It was clear from photographs, however, that a wake develops out of this bifurcation, moves towards the cathode and persists as a trail of slower-moving plasma along the cathode. It was also clear from limited single point interferometry that the wake is of significant density compared with the sheet (typically ≈50%). What was lacking was a complete picture of the evolution of the density in the two structures in space and time. To this end we have completed the survey of electron number density using the interferometer and the techniques described in this paper.

Because of the problems of the interferometer in accurately capturing the density when the rise rate was too high, which was described in section 5.1, and because of the difficulty of aligning the laser very close to the electrodes, the measurement region of this study was more limited than for the magnetic measurements. Referring to figure 8, the useable data (for an argon, 100 mTorr discharge) spanned rows 2–5, columns 25–60 for row 2 and columns 9–60 for rows 3–5, for a total of 192 measurement points. The repeatability of each measurement was estimated from many repeated measurements to be about ±10%. Due to the dynamic nature of the sheet, there are differences from shot to shot in the peak density, the arrival time and the geometry of sheet structures. This is especially true at later times in the discharge when differences from shot to shot can cause relatively large variation in the location of the sheet. Thus, the contours of density,

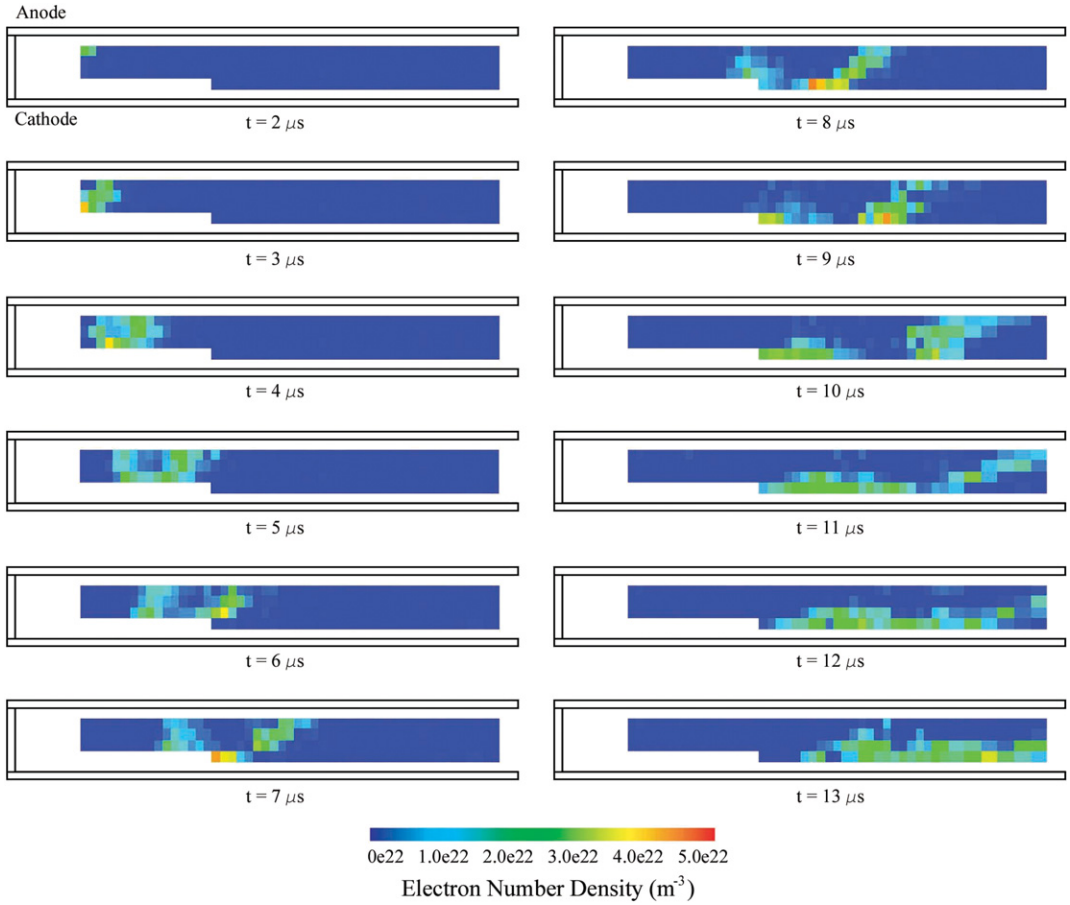

Figure 10. Electron number density contours for argon, 100 mTorr, for 2–13 μs.
(This figure is in colour only in the electronic version)

shown in figure 10 for the initial conditions of argon propellant at 100 mTorr, have less spatial resolution and repeatability than the current density contour of figure 9. Nonetheless, the density contours are valuable for showing the evolution of the sheet and wake structures.

The electron number density contours confirm the conclusions drawn from photographs and current density contours, and add additional insight as well. By four microseconds, it was clear from photographs and current density contours [6, 7] that the branch has canted ahead almost fully. The current is being carried in the canted branch, with just a trace of the trunk path of current remaining. Also, the photographs show a hook-like plasma structure behind the sheet. The bifurcation of the sheet is visible in figure 10 at 4 and 5 μs. This shows that the two initial current carrying structures (branch and trunk) are also plasma structures of comparable density. As expected, though, while the remnant of the trunk ceases to carry current after a few microseconds, the trailing plasma structure remains.

By seven or eight microseconds, the current density contours show a fully canted structure. The current has only one path of conduction now, and there is no hint of a second current carrying structure. In figure 10, the remnant of the trunk has become the wake that was previously seen in photographs. We see that this wake is of comparable density to the sheet. Furthermore, as was also shown by the photographs, the wake moves more slowly than the sheet and continues to grow longer, implying that it is being fed by mass leakage from the sheet. Together the magnetic field, current density, electron number density and photography diagnostics paint a full picture of the evolution of the branch and trunk current structures into the canted sheet and wake plasma structures. This effect is an important inefficiency of gas-fed pulsed plasma thrusters [1] and understanding the development of the wake may help to improve the performance of these accelerators.

7. Conclusions

We have presented the use of a helium–neon laser interferometer to measure the electron number density in a propagating current sheet and its wake. The experimental apparatus is somewhat unique in its suitability for use with this interferometer because of the high density and fast propagation. However, we found that in some regions of the accelerator the rise rate of density was too quick for our phase detection circuitry, leading to erroneous results. The remaining regions were probed in multiple shots in an argon discharge at 100 mTorr, and the laser beam position was changed between shots by using a moving mirror assembly. The resulting spatial maps of density allow a visualization of the evolution of the sheet and wake structures. These measurements confirm earlier descriptions of the sheet and wake dynamics, show that

the wake originates out of a bifurcation of the sheet and clearly indicate that the wake is of significant density compared with the sheet.

Acknowledgments

The authors would like to thank Bob Sorenson for his help in constructing the phase detection circuitry. This work was supported by the Air Force Office of Scientific Research and by the Program in Plasma Science and Technology of the Princeton Plasma Physics Laboratory.

References

[1] Berkery J W and Choueiri E Y 2006 *Plasma Sources Sci. Technol.* **15** 64–71
[2] Okada S, Kiso Y, Goto S and Ishimura T 1989 *J. Appl. Phys.* **65** 4625–31
[3] Golingo R P, Shumlak U and Nelson B A 2005 *Phys. Plasmas* **12** 062505
[4] Chin-Fatt C, Goldenbaum G C, DeSilva A W, Hess R, Cote C, Filuk A, Gauvreau J L and Hwang F K 1993 *Phys. Fluids* **5** 1816–27
[5] Spanjers G G, Yadlowsky E J, Hazelton R C and Moschella J J 1995 *J. Appl. Phys.* **77** 3657–67
[6] Markusic T E, Berkery J W and Choueiri E Y 2005 *IEEE Trans. Plasma Sci.* **33** 528–9
[7] Markusic T E, Choueiri E Y and Berkery J W 2004 *Phys. Plasmas* **11** 4847–58
[8] Kristal R and Peterson R W 1976 *Rev. Sci. Instrum.* **47** 1357–9
[9] Buchenauer C J and Jacobson A R 1977 *Rev. Sci. Instrum.* **48** 769–4
[10] Jacobson A R and Call D L 1978 *Rev. Sci. Instrum.* **49** 318–20
[11] Antonsen E L, Burton R L, Spanjers G G and Engelman S F 2003 *Rev. Sci. Instrum.* **74** 88–93